

Bogoliubov - de Gennes versus Quasiclassical description of Josephson structures

M. Ozana, A. Shelankov*, and J. Tobiska

Department of Theoretical Physics, Umeå University, 901 87 Umeå, Sweden

(Dated: 15 December 2001)

The applicability of the quasiclassical theory of superconductivity in Josephson multi-layer structures is analyzed. The quasiclassical approach is compared with the exact theory based on the Bogoliubov - de Gennes equation. The angle and energy resolved (coarse-grain) currents are calculated using both techniques. It is shown that the two approaches agree in $SIS'IS''$ geometries after the coarse-grain averaging. A quantitative discrepancy, which exceeds the quasiclassical accuracy, is observed when three or more interfaces are present. The invalidity of the quasiclassical theory is attributed to the presence of closed trajectories formed by sequential reflections on the interfaces.

PACS numbers: 74.80.Dm, 74.80.-g, 74.50.+r, 74.20.Fg

Studying charge current through weak links, the Josephson effect, is one of the most important part of superconductivity, both theory and experiment^{1,2}. Besides general interest, this problem is important for engineering the numerous devices based on the Josephson effect. The Josephson effect reveals itself in tunneling junctions as well as more complex mesoscopic structures built of superconducting and normal layers. A major part of the theoretical results in this field has been obtained using the method of quasiclassical Green's functions^{3,4,5,6,7}. The advantage of this general method is that disorder and inelastic processes can be conveniently incorporated into the theory. In a ballistic case, one can apply a more simple technique^{8,9} based on the Bogoliubov - de Gennes (BdG) equation¹⁰. A strong side of the BdG-approach is that it is valid for description of the interface reflection and transmission, where the potential varies on a microscopic length and the quasiclassical theory in its original form fails. As shown by Zaitsev¹¹, an isolated partially transparent interface can be taken into account by a proper boundary condition for the quasiclassical Green's functions. Recently, there has been considerable technical progress where the boundary condition is formulated using the Schopohl-Maki parameterization¹² of the quasiclassical Green's function¹³, or in terms of effective wave functions^{14,15}. However, it has been argued^{16,17} that these boundary conditions may give a wrong result in the case when a coherent scattering by several interfaces takes place. It is shown in Ref.¹⁶ that the quasiclassical density of states of a SS' sandwich disagrees with the "exact" one, found from the Gor'kov equation. The disagreement has been attributed in Ref.¹⁷ to the presence of closed trajectories formed by sequential reflections by the interface and the outer boundaries of the sandwich. In particular, the correction to the quasiclassical Green's function due to the loop-like trajectories violates the normalization condition, which is an essential element of the quasiclassical technique. In this paper, we extend these results to the case of an open geometry and analyse applicability of the quasiclassical theory to the Josephson effect in a multi-layer mesoscopic structure.

The quasiclassical theory is a simplified version of the "exact" theory of superconductivity based on the

Gor'kov Green's function formalism. The main assumption made in the course of its derivation is that the potentials vary slowly on the Fermi wave length $\lambda_F = 2\pi/p_F$, p_F being the Fermi momentum, that is the parameter λ_F/ξ_0 is small, where ξ_0 is the coherence length ($\xi_0 \sim v_F/\Delta$, v_F is the Fermi velocity). The question we address in this paper is whether there are corrections to the theory which are not controlled by the quasiclassical parameter $\lambda_F/\xi_0 \ll 1$.

To judge if the quasiclassical approach gives valid results, we compare its predictions with the solution to the BdG equation. In the clean case of the mean-field theory, the BdG approach is fully equivalent to the Green's function method, which is the starting point to the derivation of the quasiclassical approximation. For this reason we consider the BdG solutions as "exact" for the purpose of the comparison. More specifically, we consider a multi-layer $SS'S'' \dots$ structure shown in Fig.1 and calculate the angle and energy resolved partial current $j(\theta, \varepsilon)$, where θ is the angle of incidence and ε is the energy of the excitation propagating through the multi-layer structure. Comparing the results of the two approaches, we make our conclusions on the validity of the quasiclassical approximation.

As discussed in detail in Ref.^{16,17}, one cannot make any conclusions comparing directly $j_{BdG}(\theta, \varepsilon)$, evaluated from the BdG-equation with its quasiclassical counterpart $j_{qc}(\theta, \varepsilon)$. The point is that in the BdG approach, the incident particle is taken as a plane wave with precisely defined wave vector whereas in the quasiclassical approach one deals with classical trajectories, where the momentum in the direction perpendicular to the velocity has quantum uncertainty. The infinitely extended plane wave suffers multiple reflections on the interfaces, and the reflected/transmitted waves inevitably interfere because of the infinite extension. The interference leads to an intricate picture of Fabry-Perot like resonances and a fine structure in the angle dependence on the scale $\delta\theta \sim \lambda_F/a$ where a is the layer width. To illustrate this point, we show in Fig. 2 angle-energy resolved j_{BdG} current through a SISIS-system of superconductors (S) separated by two barriers (I) in a narrow region of angles (the BdG calculations are done by the method presented

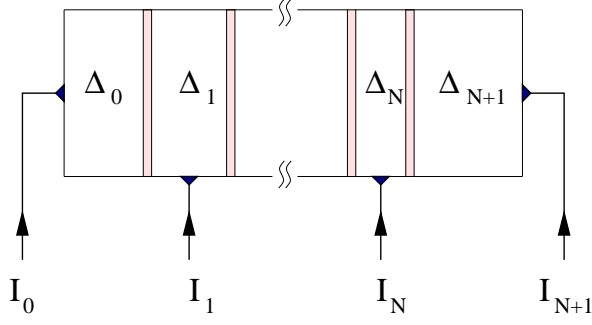


FIG. 1: A planar, multi-layer structure consisting of N layers separated by barriers and sandwiched by half-infinite electrodes. The complex order parameter denoted $\Delta_0, \dots, \Delta_{N+1}$ are considered as inputs. It is assumed that each layer is connected to an independent current source I_0, I_1, \dots so that one achieves any given distribution of the phase of the order parameters without violation of the current conservation.

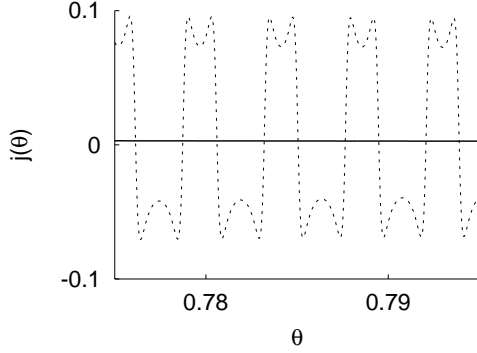


FIG. 2: Angle resolved current in a SISIS structure as a function of angle θ . The energy $\varepsilon = 1.2\Delta_0$. The order parameter in the leftmost superconductor is Δ_0 . The order parameters in the next layers read $\Delta_1 = e^{i\pi/4}\Delta_0, \Delta_2 = i\Delta_0$. The thickness of the internal layer is $a = v_F/\Delta_0$. The interface transparencies $T_1 = 0.1, T_2 = 0.5$. The dashed and solid lines show the BdG j_{BdG} and the quasiclassical current j_{qc} , respectively.

below, see also¹⁸). The “exact” current shows rapid and strong fluctuations in the region where the quasiclassical current is almost a constant. However, on a large scale of angles, j_{BdG} averaged in a small angle window (coarse-grain current) is a smooth function. As discussed in^{16,17}, the coarse-grain averaging is equivalent to building stationary wave packets, peaked on classical trajectories, on which the quasiclassical theory is formulated. It is on this low resolution level where the quasiclassical and exact theory are expected to agree with each other. For these reasons, we use only coarse-grain BdG-current for comparison with the quasiclassical theory. For definiteness, we calculate the current at the leftmost interface of the multi-layer structure.

In principle, the coarse-grain averaging can be performed analytically applying the path length expansion method of Ref.¹⁷. (In case of a double-layer, the averaging can be done directly with the result expressed via

the elliptic integrals^{19,20}.) Nevertheless, we perform the averaging by a numerical integration to avoid lengthy algebra.

The paper is organized as follows. In Sect.I we discuss solutions to the Bogolubov - de Gennes equation. In Sect.IA, we build plane waves and then, in Sect.IB, we introduce the scattering S-matrix. In Sect. IC, we express the BdG current via the elements of the S-matrix. The method which we use to evaluate the current in the quasiclassical technique is presented in Sect.II. Numerical results are shown in Sect. III, and their interpretation is presented in Sect.IV. In Sect.V we discuss validity of our results in more realistic models. Technical details of the derivation are collected in Appendices.

I. BOGOLUBOV-DE GENNES EQUATION

In this section, we consider the theory of multi-layer structure in the framework of the Bogoliubov - de Gennes equation. Stationary two-component wave function $\psi(\mathbf{r}) = \begin{pmatrix} u \\ v \end{pmatrix}$ of an excitation with the energy E satisfies the BdG-equation¹⁰, $\hat{H}\psi = E\psi$,

$$\hat{H} = \begin{pmatrix} \xi(\mathbf{p} - \frac{e}{c}\mathbf{A}) + V & \Delta \\ \Delta^* & -\xi(\mathbf{p} + \frac{e}{c}\mathbf{A}) - V \end{pmatrix} \quad (1.1)$$

where $\xi(\mathbf{p}) = \frac{\mathbf{p}^2}{2m} - \frac{p_F^2}{2m}$, p_F being the Fermi momentum, $V(\mathbf{r})$ is the potential energy, $\Delta(\mathbf{r})$ is the complex order parameter, and $\mathbf{A}(\mathbf{r})$ is the magnetic vector potential.

The charge current density \mathbf{J} can be found as

$$\mathbf{J} = \Re \left(\psi^\dagger \hat{\mathbf{J}} \psi \right) \quad (1.2)$$

where $\hat{\mathbf{J}} = -c \frac{\partial \hat{H}}{\partial \mathbf{A}}$ is the current operator

$$\hat{\mathbf{J}} = \frac{e}{m} \left(\mathbf{p} - \hat{\tau}_z \frac{e}{c} \mathbf{A} \right), \quad (1.3)$$

τ_z being the Pauli matrix.

The non-diagonal elements of current operator $\hat{\mathbf{J}}(\mathbf{r})$, $\langle \psi_n | \hat{\mathbf{J}}(\mathbf{r}) | \psi_{n'} \rangle$ are evaluated as

$$\langle \psi_n | \hat{\mathbf{J}}(\mathbf{r}) | \psi_{n'} \rangle = \frac{1}{2} \left(\hat{\mathbf{J}} \psi_n \right)^\dagger \psi_{n'} + \frac{1}{2} \psi_n^\dagger \left(\hat{\mathbf{J}} \psi_{n'} \right); \quad (1.4)$$

In superconductors, the charge current created by an elementary excitation in a state ψ_n is not a conserving quantity, *i.e.* $\text{div} \mathbf{J}_{nn} \neq 0$. The charge conservation is restored after the summation over all the BdG excitations, provided the pair potential Δ is self-consistent.

To take advantage of the unitarity property, one considers the conserving *quasiparticle* current, $\hat{\mathbf{j}}^{\text{qp}}(\mathbf{r})$, calculated with the help of the operator, $\hat{\mathbf{j}}^{\text{qp}} = \frac{\partial \hat{H}}{\partial \mathbf{p}}$, that is

$$\hat{\mathbf{j}}^{\text{qp}} = \frac{1}{m} \left(\hat{\tau}_z \mathbf{p} - \frac{e}{c} \mathbf{A} \right), \quad (1.5)$$

and

$$\mathbf{j}^{\text{qp}}(\mathbf{r}) = \Re \psi^\dagger \hat{\mathbf{j}}^{\text{qp}} \psi. \quad (1.6)$$

The continuity equation

$$\text{div } \mathbf{j}^{\text{qp}} = 0. \quad (1.7)$$

follows from the BdG equation.

We solve the BdG equation for the case of a planar structure shown in Fig.1. It is composed of N layers surrounded by two half-infinite homogeneous superconductors. The complex order parameters in each layer is a constant which is taken as an independent input.

Choosing the x axis perpendicular to the layer plane, the partially transparent interfaces are modelled by the δ -function barrier

$$V = \frac{\lambda}{m} \delta(x), \quad (1.8)$$

where λ is the strength of the potential, m is the mass. Below, we characterize the interface by the parameters $R = |\lambda/(p_F + i\lambda)|^2$ and T ($R + T = 1$) which have the meaning of the reflection coefficient (R), and transparency (T) for the normal incidence.

A. Plane wave solutions

Due to the in-plane translational invariance, the solutions can be taken in the following form

$$\Psi(\mathbf{r}; \mathbf{p}_{||}) = e^{i\mathbf{p}_{||} \cdot \mathbf{r}} \psi(x), \quad (1.9)$$

where $\mathbf{p}_{||}$ is the in-plane momentum, and ψ obeys the one-dimensional BdG equation.

First, we consider the plane wave solution to the BdG equation in each of the layers where $\Delta = \text{const}$ and $V = 0$. The function $\psi(x)$ satisfies the equation

$$\begin{pmatrix} \hat{\xi}_x & \Delta \\ \Delta^* & -\hat{\xi}_x \end{pmatrix} \psi(x) = E \psi(x), \quad (1.10)$$

where $\hat{\xi}_x = (\hat{p}_x^2 + \mathbf{p}_{||}^2 - p_F^2)/2m$, and $\hat{p}_x = -i d/dx$. Eq.(1.10) has 4 linearly independent plane wave solutions:

$$\psi_{\nu\sigma}(x) = e^{i\sigma p_\nu x} \psi_\nu, \quad \nu = \pm, \quad \sigma = \pm \quad (1.11)$$

where the momentum p_ν is found from (see Fig. 3)

$$p_\nu = \sqrt{\mathbf{p}_F^2 - \mathbf{p}_{||}^2 \pm 2m\xi}, \quad \Re p_\pm > 0 \quad (1.12)$$

with

$$\xi = \sqrt{E^2 - |\Delta|^2}. \quad (1.13)$$

We choose the branch of the square root so that $\xi > 0$ at $E > |\Delta|$ and $\Im \xi > 0$ when $E < |\Delta|$

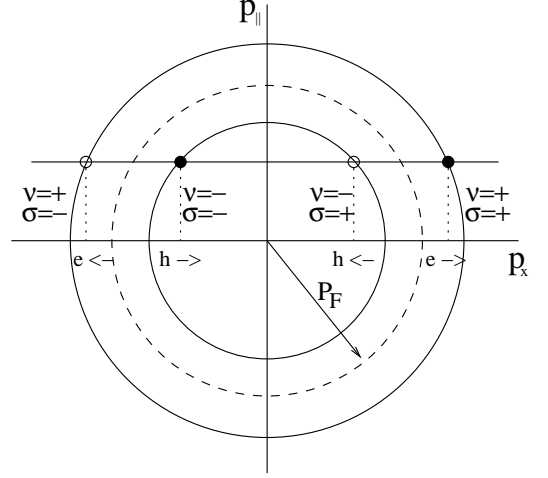


FIG. 3: 4 linearly independent solutions to BdG equation. Index ν describes the type of the quasiparticle $\nu = +$ is the electron-like and $\nu = -$ the hole-like excitation; σ defines the sign of the x -component of the momentum. As shown by arrows, the excitation propagates to the right if $\nu \cdot \sigma = +1$, and to the left otherwise.

The two-component amplitudes ψ_\pm found from Eq. (1.10) with $\hat{\xi}_x$ substituted for ξ , may be chosen in the following form

$$\psi_+ = \frac{1}{c} \begin{pmatrix} 1 \\ a \end{pmatrix} \quad ; \quad \psi_- = \frac{1}{c} \begin{pmatrix} b \\ 1 \end{pmatrix} \quad (1.14)$$

where

$$a = \frac{\Delta^*}{E + \xi}, \quad b = \frac{\Delta}{E + \xi}, \quad c = \sqrt{\frac{2\xi}{E + \xi}}, \quad (1.15)$$

($c = \sqrt{1 - ab}$). These expressions are applicable for any energy E including the gap region $E < |\Delta|$. Outside the gap, $b = a^*$.

The amplitudes are normalized to the unit flux, *i.e.*

$$\psi_\pm^\dagger \hat{\tau}_z \psi_\pm = \pm 1, \quad E > |\Delta|. \quad (1.16)$$

Note the orthogonality relation (outside the gap), $\psi_\pm^\dagger \hat{\tau}_z \psi_\mp = 0$, in agreement with the current conservation in Eq. (1.7). For any E , the determinant of the matrix $[\psi_+, \psi_-]$ the columns of which are ψ_+ and ψ_- , equals to unity (in other words, $\psi_+^T i \hat{\tau}_y \psi_- = 1$).

For future needs, we define conjugated amplitudes ψ_ν^\dagger ,

$$\psi_\nu^\dagger \equiv -\nu \psi_{-\nu}^T i \hat{\tau}_y, \quad (1.17)$$

which possesses useful properties of orthonormality and completeness:

$$\psi_\nu^\dagger \psi_{\nu'} = \delta_{\nu\nu'}, \quad \sum_\nu \psi_\nu \psi_\nu^\dagger = \hat{1} \quad (1.18)$$

where $\hat{1}$ is the unit 2×2 matrix. Outside the gap, where $\psi_\nu^\dagger = \nu \psi_\nu^\dagger \hat{\tau}_z$, the orthonormality expresses the quasiparticle current conservation.

The physical meaning of the quantum numbers ν and σ is clear: in accordance with the sign of the probability flux Eq. (1.16), the excitations with $\nu = 1$ are electron-like whereas the states $\nu = -1$ are hole-like. The parameter σ shows the direction of the momentum. The excitations for which the product $\sigma\nu$ equals to $+1$ (-1) propagate in the positive (negative) direction of the x -axis.

B. The scattering matrix

To introduce the scattering matrix, we first define the in-coming and out-going free states, the amplitudes of which are related by the S-matrix. We number the in-coming plane wave states in the following way:

$$\begin{aligned} |1\rangle_{\text{in}}^{(0)} &= \Psi_{++}^{(L)} & , & & |2\rangle_{\text{in}}^{(0)} &= \Psi_{--}^{(L)} \\ |3\rangle_{\text{in}}^{(0)} &= \Psi_{+-}^{(R)} & , & & |4\rangle_{\text{in}}^{(0)} &= \Psi_{-+}^{(R)} . \end{aligned} \quad (1.19)$$

As before, the first of the lower indices of Ψ 's specifies the electron-hole degree of freedom ("+" for electron, and "-" for hole) and the second one shows the direction of the momentum $\sigma = \pm$; the upper index L or R specifies the initial location of the excitation on the left or right side of the structure. The out-going states are

$$\begin{aligned} |1\rangle_{\text{out}}^{(0)} &= \Psi_{+-}^{(L)} & , & & |2\rangle_{\text{out}}^{(0)} &= \Psi_{-+}^{(L)} \\ |3\rangle_{\text{out}}^{(0)} &= \Psi_{++}^{(R)} & , & & |4\rangle_{\text{out}}^{(0)} &= \Psi_{--}^{(R)} . \end{aligned} \quad (1.20)$$

The basis wave function read

$$\Psi_{\nu\sigma} = \sqrt{\frac{m}{2\pi p_\nu}} e^{i\sigma p_\nu x + i\mathbf{p}_\parallel \cdot \mathbf{r}} \psi_\nu , \quad (1.21)$$

with ψ_ν from Eq. (1.14), these function are normalised to $\delta(\mathbf{p}_\parallel - \mathbf{p}'_\parallel) \delta(E - E')$.

In the L- or R-regions of free motion, the solution to the BdG equation, $|i\rangle$, corresponding to the incident quasiparticle in the state $|i\rangle_{\text{in}}^{(0)}$ can be presented as

$$|i\rangle = |i\rangle_{\text{in}}^{(0)} + \sum_{f=1}^4 S_{fi} |k\rangle_{\text{out}}^{(0)} . \quad (1.22)$$

These equations with $i = 1, \dots, 4$ define the 4×4 S-matrix. The method which allows us to evaluate the elements of S-matrix is presented in Appendix A.

C. The BdG current

Expressed via the distribution function of the excitations $n_i(E)$, (where E is the energy and $i = 1, \dots, 4$ and E is the quantum number introduced in Eq. (1.22)), the charge current in the x -direction reads¹⁰

$$J(x) = \int d\mathbf{p}_\parallel \int_0^\infty dE \sum_{i=1}^4 (2n_i(E) - 1) \langle i, E | \hat{J}(x) | i, E \rangle , \quad (1.23)$$

$\hat{J}(x)$ being the current operator Eq. (1.3). We restrict ourself to the simplest case where the distribution function depends only on energy, *i.e.* $n_i(E) = n(E)$. Then, the current can be written as

$$J(x) = \int d\mathbf{p}_\parallel \int_0^\infty dE (2n(E) - 1) J(E, \mathbf{p}_\parallel; x) \quad (1.24)$$

where the partial current density, $J(E, \mathbf{p}_\parallel; x)$ at the point x , is

$$J(E, \mathbf{p}_\parallel; x) = \sum_{i=1}^4 \langle i, E | \hat{J}(x) | i, E \rangle \quad (1.25)$$

To evaluate the current in the left or right electrodes, we substitute $|i\rangle$ from Eq. (1.22), and take into account the unitarity property, $\sum_{i=1}^4 S_{f'i}^* S_{fi} = \delta_{f'f}$. We get

$$J(E, \mathbf{p}_\parallel; x) = J_E^{(0)}(x) + 2\Re \sum_{i,f=1}^4 S_{fi}^* J_{fi}^{(0)}(x) \quad (1.26)$$

where $J_E^{(0)}(x) = \sum_{k=1}^4 J_{kk}(x)$: here summation is performed over the 4 plane wave states Fig. 3 on the left or right side of the structure. The meaning of $J_E^{(0)}$ is that it would give the (partial) current in the left or right region if the plane wave states with the given energy E were equally occupied. This is the contribution to the current which produces the bulk supercurrent $2eN_s \mathbf{v}_s$. In our case, $J_E = 0$ since the phase of the order parameter is assumed to be a constant within the outside regions.

The second term in the right hand side of Eq. (1.26) is due to the interference of the incoming and outgoing waves. Considering for definiteness the left region, the initial states $i = 1, 2$ interfere with the final $f = 3, 4$ states. For the energy E outside the gap, $J_{fi}^{(0)}$ is other than zero only if $i = 1, f = 2$ or $i = 2, f = 1$ (*i.e.* for the interference with the Andreev reflected particle). The partial current density $J(E, \mathbf{p}_\parallel)$ at the point adjacent to the first interface, *i.e.* at $x = 0^-$ reads

$$J(E, \mathbf{p}_\parallel) = 2\Re \left(S_{21}^* J_{41}^{(0)}(0^-) + S_{12}^* J_{32}^{(0)}(0^-) \right) . \quad (1.27)$$

Calculating the current matrix elements Eq. (A3) with the amplitudes in Eqs. (1.14), and (A8), one derives from Eq. (1.27) that

$$J(E, \mathbf{p}_\parallel) = \frac{1}{\pi} \Re \frac{1}{\xi} (S_{21} \Delta_0 - S_{12} \Delta_0^*) \quad , \quad E > |\Delta_0| . \quad (1.28)$$

where Δ_0 is the order parameter in the left electrode (see Fig. 1)²¹. The scattering matrix is calculated by the transfer matrix method as described in Section A.

Eq. (1.28) gives the BdG current carried by plane wave states with definite value of \mathbf{p}_\parallel . This quantity strongly

fluctuates (see e.g. Fig. 2) as a function of the incidence angle θ , $p_{||} = p_F \sin \theta$ in the region $\Delta\theta \sim 1/(p_F a)$, a being typical interlayer distance. To come to the trajectory-like picture, one performs averaging in a region of angles $\sim \Delta\theta$. It is the coarse-grain current which should be compared with the current density found from the quasiclassical technique.

II. QUASICLASSICAL CURRENT

In the quasiclassical technique,, the current density \mathbf{j} reads⁴:

$$\mathbf{j} = \int d\varepsilon \frac{d\Omega_{\mathbf{n}}}{4\pi} \mathbf{j}_{\mathbf{n}}(\varepsilon) (1 - 2n(\varepsilon)) , \quad (2.1)$$

where ε is energy and \mathbf{n} a unit vector which shows the direction of the momentum, $n(\varepsilon)$ is the distribution function, and the angular and energy resolved current $\mathbf{j}_{\mathbf{n}}(\varepsilon)$ is found as

$$\mathbf{j}_{\mathbf{n}}(\varepsilon) = v_F \mathbf{n} \operatorname{Re} (g_{\mathbf{n}}^R(\varepsilon))_{11} , \quad (2.2)$$

where v_F is the Fermi velocity and $g_{\mathbf{n}}^R$ is the retarded quasiclassical Green's function (see e.g. Ref.¹⁴ for notation). For a given energy ε and a parallel momentum $p_{||}$, the x component of the current along the x axis is sum of the contributions $j_{\mathbf{n}_1} + j_{\mathbf{n}_{1'}}$, where $(\mathbf{n}_1)_x = \cos \Theta$ and $(\mathbf{n}_{1'})_x = -\cos \Theta$ with Θ being the angle of the trajectory defined as $\sin \Theta = p_{||}/p_F$. In order to compare the current with Eq. (1.28), we change the integration in Eq. (2.1) as follows: $\int d\Omega_{\mathbf{n}} \leftrightarrow \int dp_{||}/p_F$ and $\int_{-\infty}^{\infty} d\varepsilon \leftrightarrow 2 \int_0^{\infty} d\varepsilon$. The corresponding partial current then reads

$$j_{p_{||}}(\varepsilon) = v_F \frac{p_{||}}{p_F} \operatorname{Re} (g_{\mathbf{n}_1}^R - g_{\mathbf{n}_{1'}}^R)_{11} , \quad (2.3)$$

$$\mathbf{j} = \int_0^{\infty} d\varepsilon \int_0^{\infty} \frac{dp_{||}}{p_F} j_{p_{||}}(\varepsilon) (1 - 2n(\varepsilon)) , \quad (2.4)$$

where the Green's functions are taken at the same space point, e.g. at the interface shown on Fig.4a.

To evaluate the Green's function g ($= g^R$), we use the method of Ref. 14,16 and express the 2×2 matrix g via two-component "wave functions" ϕ_{\pm} on classical trajectories:

$$g = \frac{2}{N} \phi_+ \bar{\phi}_- - 1 \quad ; \quad N = \bar{\phi}_- \phi_+ , \quad (2.5)$$

where $\bar{\phi} = -i\phi^T \tau_y$. These amplitudes obey Andreev-like equation on classical trajectories (see^{14,16}). The index \pm denotes solutions with different asymptotic behaviour: the amplitude $\phi_+ \rightarrow 0$ for the trajectory coordinate x going to $+\infty$: $x \rightarrow \infty$, and $\phi_- \rightarrow 0$ for $x \rightarrow -\infty$.

The Andreev equation needs a boundary condition when the trajectory hits an interface and ballistic pieces of trajectories are tied by a "knot", see Fig.4a. The

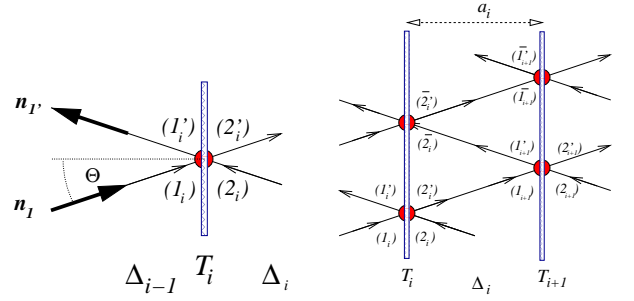


FIG. 4: (a) The multi-layer structure consisting of N superconducting layers surrounded by 2 half-infinite superconductors. The order parameters are $\Delta_0, \dots, \Delta_{N+1}$, the interface transparencies are T_1, \dots, T_{N+1} , and the thicknesses of the layers a_1, \dots, a_N . (a) Scattering on the i 'th interface with the transparency T_i . The angle of the trajectory is Θ . (b) The zig-zag trajectory inside of i 'th superconducting layer with the order parameter Δ_i . Due to the translational symmetry are certain parts of the trajectory equivalent, e.g. $1 \leftrightarrow \bar{1}$, $2 \leftrightarrow \bar{2}$, \dots .

boundary condition can be formulated via the transfer matrix $M_{j' \leftarrow j}$ ¹⁴,

$$\phi_{j'} = M_{j' \leftarrow j} \phi_j . \quad (2.6)$$

which relates the wave function on the incoming trajectory j to that on the outgoing trajectory j' ; here and below, j denote incoming channels, whereas j' is the outgoing reflected one, e.g. $j = 1_i$ and $j' = 1'_i$ on Fig.4a. The "knot" transfer matrix $M_{j' \leftarrow j}$ is expressed in terms of "across knot" Green's function $g_{k' \bullet k}$ which depends on the amplitudes ϕ_{\pm} in the channels on the other side of the interface¹⁴

$$M_{1'_i \leftarrow 1_i} = \frac{1+R}{2r^*} \left(1 - \frac{T}{1+R} g_{2'_i \bullet 2_i} \right) , \quad (2.7)$$

$$g_{2'_i \bullet 2_i} = \frac{2}{N} \phi_{(2'_i)+} \bar{\phi}_{(2_i)-} - 1 , \quad (2.8)$$

$$N = \bar{\phi}_{(2_i)-} \phi_{(2'_i)+} , \quad (2.9)$$

where T and $R = |r|^2$ are the transmission and the reflection probabilities. The indices 1_i and 2_i refer to the channels on the other side of an interface, see Fig.4a. According to Eq.(2.8) the "plus" amplitude ϕ_+ is needed only in the outgoing channels and the "minus" amplitude ϕ_- in the incoming ones.

In order to find the Green's function in one of the external channels (channels which lead to the infinity) we need to calculate the amplitudes $\phi_{(j)+}$ and $\phi_{(j')-}$ in the channels inside of the structure. To find these amplitudes it is convenient to introduce the total transfer matrix \mathcal{M} . If one considers the periodic zig-zag trajectory inside of i 'th layer, see Fig.4b the \mathcal{M} is defined as the operator connecting the corresponding parts, for example the trajectories (2_i) and $(\bar{2}_i)$ or $(2'_i)$ and $(\bar{2}'_i)$. The total transfer matrices in the i 'th layer shown on Fig.4b read

$$\mathcal{M}_{\bar{2}_i \leftarrow 2_i} = U_i M_{1'_i \leftarrow 1_i} U_i M_{2'_i \leftarrow 2_i} , \quad (2.10)$$

$$\mathcal{M}_{\bar{2}_i \leftarrow 2'_i} = \mathcal{M}_{\bar{2}_i \leftarrow \bar{2}_i} \mathcal{U}_i \mathcal{M}_{1'_{i+1} \leftarrow 1_{i+1}} \mathcal{U}_i, \quad (2.11)$$

$$\mathcal{U}_i = \mathbb{1} \cos \frac{\xi_i a_i}{v_F \cos \Theta} + i \hat{g}_0 \sin \frac{\xi_i a_i}{v_F \cos \Theta} \quad (2.12)$$

$$\hat{g}_0 = \frac{1}{\xi_i} \begin{pmatrix} \varepsilon & -\Delta_i \\ \Delta_i^* & -\varepsilon \end{pmatrix}, \quad (2.13)$$

where \mathcal{U}_i is the propagator across the i 'th layer¹⁴, $\xi_i^2 = \varepsilon^2 - |\Delta_i|^2$, $\text{Im} \xi_i > 0$ and $\mathcal{M}_{j' \leftarrow j}$ is the “across knot” transfer matrix. The transfer matrices $\mathcal{M}_{\bar{1}_{i+1} \leftarrow 1_{i+1}}$ and $\mathcal{M}_{\bar{1}'_{i+1} \leftarrow 1'_{i+1}}$ are found in the same way. As shown in Ref.¹⁴ the quasiclassical Green's function is found as

$$g_j = \frac{\mathcal{M}_{\bar{j} \leftarrow j} - \mathbb{1} \frac{1}{2} \text{Tr} \mathcal{M}_{\bar{j} \leftarrow j}}{\sqrt{(\mathcal{M}_{\bar{j} \leftarrow j} - \mathbb{1} \frac{1}{2} \text{Tr} \mathcal{M}_{\bar{j} \leftarrow j})^2}}. \quad (2.14)$$

For example if we want to calculate Green's function in the channel (2_i) we first find the total transfer matrix $\mathcal{M}_{\bar{2}_i \leftarrow 2_i}$ connecting ϕ 's in channels (2_i) and $(\bar{2}_i)$ and then we calculate $g_{(2_i)}$ from Eq.(2.14).

When the quasiclassical Green's functions $g_{(2_i)}$, $g_{(2'_i)}$, $g_{(1_{i+1})}$ and $g_{(1'_{i+1})}$ are known in each layer, one can invert Eq.(2.5) and calculate the amplitudes $\phi_{(2_i)-}$, $\phi_{(2'_i)+}$, $\phi_{(1_{i+1})-}$ and $\phi_{(1'_{i+1})+}$:

$$\phi_{(j')-} = \begin{pmatrix} 1 - (g_{j'})_{22} \\ (g_{j'})_{21} \end{pmatrix}, \quad (2.15)$$

$$\phi_{(j)-} = \begin{pmatrix} -(g_j)_{12} \\ 1 - (g_j)_{22} \end{pmatrix}. \quad (2.16)$$

Using Eqs.(2.5-2.16) we can write down the following iterative procedure:

1. Set all the knot values of the amplitudes ϕ_- in the incoming channels and ϕ_+ in the outgoing channels to the bulk values

$$\phi_{(1'_i)+} = \phi_{(2'_i)+} = \begin{pmatrix} 1 \\ \frac{\Delta_i^*}{\varepsilon + \xi_i} \end{pmatrix}, \quad (2.17)$$

$$\phi_{(1_i)-} = \phi_{(2_i)-} = \begin{pmatrix} \frac{\Delta_i}{\varepsilon + \xi_i} \\ 1 \end{pmatrix}, \quad (2.18)$$

where Δ_i is the order parameter in the i 'th layer, and $\xi_i^2 = \varepsilon^2 - |\Delta_i|^2$.

2. Using the values of the amplitudes ϕ_{\pm} , the “across-knot” Green's functions $g_{2'_i \bullet 2_i}$ and $g_{1'_{i+1} \bullet 1_{i+1}}$ are constructed from Eq.(2.8).
3. The “across-knot” Green's functions are substituted into Eq.(2.7) to calculate the knot transfer matrices $\mathcal{M}_{j' \leftarrow j}$, where here and below index j stays for 1_i or 2_i in i 'th layer.
4. The total transfer matrices $\mathcal{M}_{\bar{j} \leftarrow j}$ and $\mathcal{M}_{\bar{j}' \leftarrow j'}$ are calculated using Eqs.(2.10-2.11) in all layers.

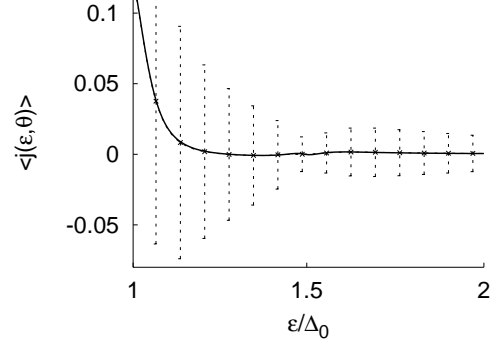


FIG. 5: Angle resolved current in SISIS structure averaged over small range of $d\theta = 0.09$ as a function of energy. The angle of incidence $\theta = \pi/4$. The solid and dashed lines show for the quasiclassical and coarse-grain BdG current, respectively. The bars show the fluctuation of the high-resolution BdG current around its average value. The order parameter in the leftmost superconductor is Δ_0 . The order parameters in the next layers read $\Delta_1 = e^{i\pi/4}\Delta_0$, $\Delta_2 = i\Delta_0$. The interface transparencies $T_1 = 0.1$, $T_2 = 0.5$. the thickness of the layer $a = v_F/\Delta_0$.

5. Using the values of the total transfer matrices from step 4. the quasiclassical Green's functions g_j and $g_{j'}$ are found from Eq.(2.14).
6. At this stage the quasiclassical Green's function g_j and $g_{j'}$ are known in all layers and the amplitudes $\phi_{(j)-}$ and $\phi_{(j')-}$ can be evaluated using Eq.(2.15-2.16).
7. Continue from point 2. until the convergence is reached.

After the last iteration the internal amplitudes $\phi_{(j)-}$ and $\phi_{(j')-}$ are known and one constructs the “knot” transfer matrix $\mathcal{M}_{1' \leftarrow 1}$ on the leftmost external interface. Since $\phi_{(1')-}$ and $\phi_{(1)-}$ are the bulk superconductor amplitudes (see Eqs.(2.17-2.18)) one calculates also the Green's functions $g_{(1)}$, $g_{(1')}$ and the partial current in Eq.(2.3).

III. RESULTS

In this section we present results of the calculations for typical parameters of the multi-layer structure such as distribution of the order parameter, thicknesses and number layers (barriers), and the strength of the barriers. Thicknesses of the layers are usually of order of v_F/Δ_0 where Δ_0 is the gap in the leftmost layer. The value $p_F = 10^3 \Delta_0/v_F$ is chosen for the Fermi momentum.

A typical high resolution angular dependence of the current $j_{BdG}(\theta)$ has been already shown in Fig. 2. As expected, it does not have any resemblance to the smooth quasiclassical behaviour. However, after the coarse grain averaging, *i.e.* on a low resolution level, j_{BdG} is in perfect

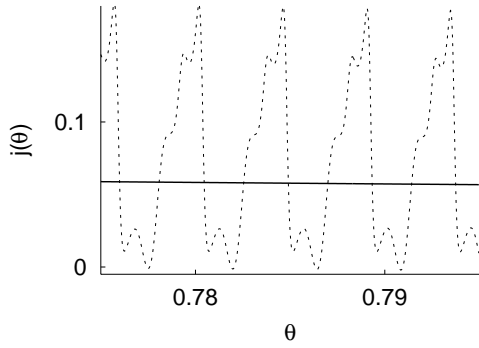


FIG. 6: Angle resolved current in a three-barrier structure SISIS as a function of angle θ as found from the BdG equation. The order parameter in the leftmost superconductor is Δ_0 . The order parameters in the next layers read $\Delta_1 = i\Delta_0, \Delta_2 = -\Delta_0, \Delta_3 = -i\Delta_0$. The thicknesses of the two internal layers $a_1 = v_F/\Delta_0, a_2 = v_F/\Delta_0$. The energy $\epsilon = 1.1\Delta_0$. The interface transparencies $T_1 = 0.1, T_2 = 0.5, T_3 = 0.5$. The solid line corresponds to the quasiclassical current, a constant in this narrow interval. The dashed line shows the BdG current.

agreement with quasiclassics, see Fig.5. The “error-bars” in Fig.5 show the mean square fluctuation of the high resolution current around its coarse-grain average. In the double-barrier case, the agreement exists for any angle θ and energy ϵ , and for any set of parameters of the structure, Δ ’s and the barrier’s strength.

Contrary, noticeable deviations from the quasiclassical solutions are seen when there are more than two barriers. Here we present results only for three-barrier structures, more complicated systems show qualitatively same features.

For a three-interface structure, a typical high resolution angle dependence of j_{BdG} is shown in Fig. 6. In Fig.7 we plot coarse-grain BdG-current together with the quasiclassical curve for slightly different geometries: Fig.7(a) refers to a symmetric case when the two internal layers have exactly the same thickness whereas in 7(b) the thicknesses are 10 percent different from each other. In the both cases, one sees a clear deviation of the quasiclassical curve from the “exact” one, the deviation lesser in asymmetric geometry.

For the same geometries and the order parameters, the energy dependence of the current integrated with respect to the incident angle are shown in Fig.8. Disagreement between the exact and quasiclassical results are clearly seen, again stronger in the symmetric case.

IV. DISCUSSION

The results of the previous section clearly show that in some geometries the quasiclassical theory does not reproduce the “exact” results derived from the BdG equation. The two approaches agree only qualitatively. The quan-

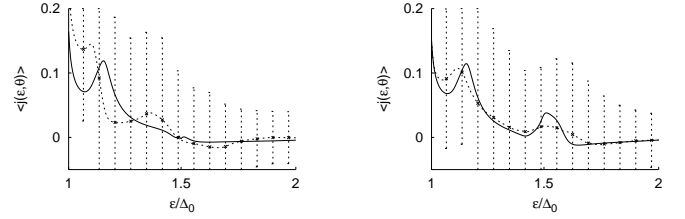


FIG. 7: (a) (b) Angle resolved current averaged over small range of $d\theta = 0.09$ as a function of energy. The angle of incidence $\theta = \pi/4$. The solid line stands for the quasiclassics and the dashed line for the BdG current. The bars show how the BdG current changes around its average value. The order parameter in the leftmost superconductor is Δ_0 . The order parameters in the next layers read $\Delta_1 = i\Delta_0, \Delta_2 = -\Delta_0, \Delta_3 = -i\Delta_0$. The interface transparencies $T_1 = 0.1, T_2 = 0.5, T_3 = 0.1$. (a) Symmetric case: the thicknesses of the two internal layers $a_1 = v_F/\Delta_0, a_2 = v_F/\Delta_0$. (b) Non-symmetric case: $a_1 = 0.9 v_F/\Delta_0, a_2 = 1.1 v_F/\Delta_0$.

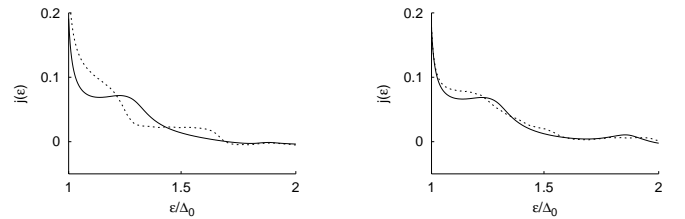


FIG. 8: (a) (b) The total current as a function of energy. The solid line stands for the quasiclassical and the dashed line for the BdG current. The order parameter in the leftmost superconductor is Δ_0 . The order parameters in the next layers read $\Delta_1 = i\Delta_0, \Delta_2 = -\Delta_0, \Delta_3 = -i\Delta_0$. The interface transparencies $T_1 = 0.1, T_2 = 0.5, T_3 = 0.1$. (a) Symmetric case: the thicknesses of the two internal layers $a_1 = v_F/\Delta_0, a_2 = v_F/\Delta_0$. (b) Asymmetric case: $a_1 = 0.9 v_F/\Delta_0, a_2 = 1.1 v_F/\Delta_0$.

titative discrepancy much exceeds the corrections to the quasiclassical theory of order of $1/p_F a \sim \Delta/p_F v_F$ which one might expect. Below, we present our understanding of physics behind the discrepancy.

As in our earlier papers^{14,16,17}, we ascribe the failure of the quasiclassical theory to the presence of interfering paths or, in other words, loop-like trajectories. From this point, the validity of the quasiclassical theory in the two-barrier case (see Fig.5) is in accordance with our expectations. Indeed, in this simple geometry, the classical path shown in Fig. 9a, is effectively one dimensional (tree-like trajectory in the terminology of Ref.¹⁴) in the sense that there is only one path connecting any two points. As discussed in Ref.¹⁴, one is then able to factorize the full propagator $G(x, x')$, x, x' labelling the points on the tree-like trajectory, as $G(x, x') = g(x, x') \exp[ip_F \mathcal{L}_{xx'}]$, where $\mathcal{L}_{xx'}$ is the length of the path along the tree-like trajectory connecting x and x' , and $g(x, x')$ is a slowly varying quasiclassical (2-point) Green’s function. In this

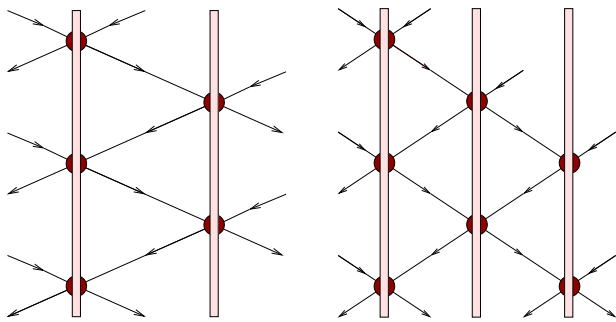


FIG. 9: (a) (b)
Classical trajectories. The trajectory is built of ballistic pieces “tied” by scattering on the two interfaces (knots). The arrows show the direction of the momentum. There are no interfering paths in a double-layer case (a). Loops exist in a three-barrier system (b).

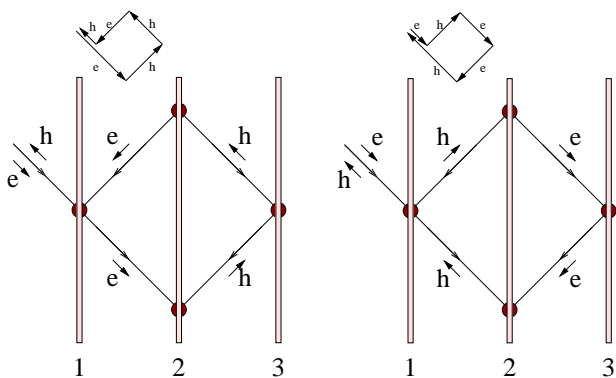


FIG. 10: (a) (b)
Simplest loop like paths contributing to the Andreev reflection amplitude in a symmetric double-barrier structure. The incoming electron comes from the left and is reflected as a hole after going around the loop anti-clockwise (a) and clockwise (b). Arrows on the continuous lines show the direction of momentum. Letters “e” and “h” show the character of the excitation – electron or hole. The arrows under the letters show the direction of propagation.

case, derivation of the quasiclassical equation does not meet any difficulty, and the theory gives valid results.

Turning now to the symmetric three-barrier structure, the trajectory is *not* simple tree-like (see Fig.9(b)): there are loops and, therefore, interfering paths. Then, one may expect corrections to the quasiclassical theory, which are not controlled by the quasiclassical parameter¹⁷. The origin of the corrections and its relation to the existence of loops, can be understood from the following semi-quantitative arguments.

In the BdG-picture the current Eq. (1.28) is expressed via the element of the S-matrix S_{12} that is the Andreev reflection amplitude $A_e \equiv S_{12}$. Scattering amplitudes can be presented as a sum of partial amplitudes, each of which corresponds to a particular path of the particle. Among others, there are closed paths shown in Fig.10. The contribution A_e^{loops} of the paths in Fig.10(a) and (b)

to the full Andreev reflection amplitude A_e is evaluated in appendix B,

$$A_e^{\text{loops}} = \mathcal{A} \Re \left(r_1 r_3^* e^{2i(\cos \theta_{pF}(a_1 - a_2))} \right) \quad (4.1)$$

where \mathcal{A} is a coefficient defined in Eq. (B5), a_1 (a_2) is the distance from the barrier 1 to barrier 2 (from 2 to 3); r_1 and r_3 are the amplitudes of reflection from the barrier 1 and 3 respectively. Note that this simplest loop survives the coarse grain averaging only if $a_1 \approx a_2$. We understand the larger deviation from quasiclassics seen in the symmetric case compared with an asymmetric one, as due to the contribution of the simple loop.

The existence and importance of this contribution can be checked exploiting the fact that it is sensitive to the phase of the reflection coefficients and the length of the path on the scale of $1/p_F$. In Fig.11, we show the current for different signs of the barrier strength $\lambda_3 = \pm|\lambda_3|$, changing the phase of $r_3 = -i\lambda_3/(p_{Fx} + i\lambda_3)$ but leaving the reflection probability intact. In Fig.12, we plot the change of the exact and quasiclassical currents upon tiny variation of the right layer thickness (corresponding to π -change of the Fermi phase factor in Eq. (4.1)). While quasiclassical current remains intact, clearly seen changes are observed in the exact current with the order of magnitude consistent with Eq. (4.1).

To avoid confusion, we remind that we deal with coarse-grain averaged currents, and therefore the observed sensitivity to the thickness and the phase of reflection has nothing to do with the size effects (due to the commensurability of the thickness and the Fermi wave length) well known in the normal case. We note also, that the loops in Fig.10 do not exist in the normal state because the electron-hole conversion on the interface 2 would not be possible.

We assert that the loop contribution Eq.(4.1) is chiefly responsible for the deviations from the quasiclassical theory. Obviously, this contribution cannot be grasped by quasiclassics since A_e^{loops} is sensitive to the phase of the reflection amplitudes r_1 and r_3 , whereas the quasiclassical boundary condition^{11,13,14} contain only the probabilities $|r|^2$ and $|t|^2$. This is our argument supporting our interpretation of the numerical results. Note that the interpretation is consistent with the observation that the deviation from quasiclassics are significantly smaller in the asymmetric case Fig.8: There, the simple loops are absent and the deviations from the conventional quasiclassics come from higher order loops (like that analysed in¹⁷).

V. CONCLUSIONS

In this paper we have examined the applicability of quasiclassical theory for description of multiple interface scattering by comparing quasiclassical solutions with “exact” ones, extracted from coarse-grain averaged solutions to the Bogoliubov - de Gennes equation. We see that the

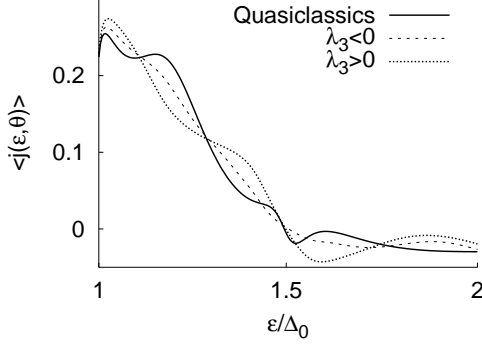


FIG. 11: Angle resolved current averaged over small range of $d\theta = 0.09$ as a function of energy. The angle of incidence $\theta = \pi/4$. The solid line stands for the quasiclassical current. The other two lines correspond to λ_3 positive or negative. The order parameter in the leftmost superconductor is Δ_0 . The order parameters in the next layers read $\Delta_1 = i\Delta_0, \Delta_2 = -\Delta_0, \Delta_3 = -i\Delta_0$. The interface transparencies $T_1 = 0.5, T_2 = 0.5, T_3 = 0.5$. The thicknesses of the two internal layers $a_1 = v_F/\Delta_0, a_2 = v_F/\Delta_0$.

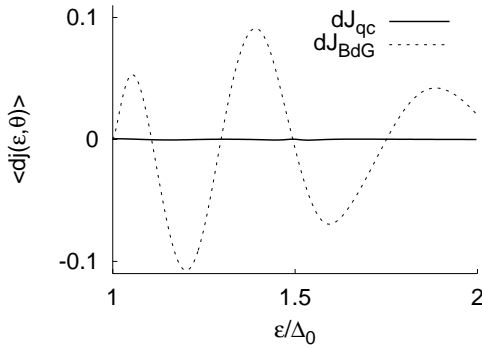


FIG. 12: The differences between currents in SSSS setups differing only by the thickness of the last layer. The thicknesses are $a_1 = a_2 = v_F/\Delta_0$ in the first case and $a_1 = v_F/\Delta_0$ and $a_2 = 1.002v_F/\Delta_0$ in the second case. The order parameter in the leftmost superconductor is Δ_0 . The order parameters in the next layers read $\Delta_1 = i\Delta_0, \Delta_2 = -\Delta_0, \Delta_3 = -i\Delta_0$. The interface transparencies $T_1 = 0.5, T_2 = 0.5, T_3 = 0.5$.

two approaches agree in simple geometries (one or two interfaces) but show noticeable discrepancy when three or more interfaces are present. This gives an example of a physical system where quasiclassical technique fails to give quantitative description with its expected accuracy $\sim 1/p_F\xi_0$. As we understand it, the failure of the quasiclassical theory occur when classical trajectories form closed loops (interfering paths) after sequential reflection and transmission accompanied by electron-hole conversion. This gives additional support to the point of view of Ref.¹⁴ that the derivation of the quasiclassical technique is possible only under the assumption of a simply connected topology, tree-like, of classical trajectories.

The main goal of this paper has been to demonstrate

the existence of noticeable deviations from the quasiclassical theory in conditions where one might expect it to give fully reliable results. For this purpose we have chosen the simplest “exact” method, the Bogoliubov - de Gennes approach, where the superconductivity enters via the mean-field order parameter $\Delta(\mathbf{r})$ and scattering due to either impurity or surface roughness is not included. It is now time to discuss to what extent our results are sensitive to the simplifications.

The truly “exact” theory of (phonon-mediated) superconductivity, for which the quasiclassical technique is an approximation, is the set of Gor’kov-Eliashberg equations for disorder averaged Green’s function \mathcal{G}_ε ²². The equation of motion, $(\varepsilon - \mathcal{H}_\varepsilon)\mathcal{G}_\varepsilon = 1$, contains the operator \mathcal{H}_ε which has the same structure as the Bogoliubov - de Gennes Hamiltonian Eq. (1.1), with the order parameter replaced by the anomalous part of the electron-phonon self-energy. Apart from the ε -dependence of \mathcal{H}_ε , the only qualitative difference is that the \mathcal{H}_ε has a non-Hermitian part coming from the self-energies. The latter accounts for the impurity and electron-phonon scattering and, correspondingly, for a finite life time of the excitation with a given momentum, $\tau(\varepsilon)$ – the scattering-out time. Due to the similarity of the above operators, the interference contribution to observables obtained with the help of the Green’s function technique or simple minded mean-field Bogoliubov - de Gennes equation, would give same results. A finite life time is the only important feature missing in the Bogoliubov - de Gennes approach, and below we discuss its role.

Clearly, the interference of waves having travelled different paths occurs if only the decay length is not too small compared with the path lengths. By virtue of the optical theorem, the waves corresponding to the ballistic trajectories decays on the distance $\sim v_F\tau$. In practice, τ is controlled by the bulk impurity scattering, so that the loops in Fig. 10 may contribute only if the interlayer distances are less or of order of the impurity mean path. As far as interface imperfection is concerned, short-range surface roughness is expected to play the role similar to that of the bulk impurity scattering: Although the interface reflection becomes partially diffusive, the coherent specular component, with the intensity proportional to the Fuchs’s parameter \mathcal{P} , is finite^{23,24}. Thus, the picture of trajectories as that shown in Fig. 10 remains meaningful as well as Eq. (4.1) if corresponding attenuation factors are inserted. We see that although microscopic roughness and bulk scattering suppress the interference effect, it survives disorder averaging if the disorder is not too strong.

When a long-range roughness is present, that is the layer thicknesses are slowly varying, the global value of the loop contribution in Eq. (4.1) averages to zero (if the thickness modulation exceeds λ_F). However, the interference of paths forming the loops is sensitive mainly to the local value of the thicknesses, so that the interference effects can be seen in the spatial fluctuations of the local current, which is a measurable quantity. In the quasiclas-

sical theory, the roughness would reveal itself only of the thickness modulation is somehow comparable with the coherence length. Since the loops are sensitive to variations of geometry on the scale of λ_F , their contribution to the fluctuations is expected to be much larger than that in the quasiclassical theory.

We see that the deviation from the quasiclassical theory due to the interference effects, although most pronounced in the idealized model exploited in the paper, are observable in realistic conditions if the disorder is not too strong. After disorder averaging, the interference contribution is observable if the mean free path exceeds the interlayer distance and the rough interfaces have not too small coefficient of the specular reflection. Detail analysis of the loop contribution to mesoscopic fluctuations is beyond the scope of the paper.

Apart from disorder, the interference contribution may be suppressed by energy integration. Indeed, the integration with the Fermi-Dirac distribution function corresponding to the temperature T is equivalent to the Matsubara summation, that is energy variable ε assumes discrete imaginary values, multiples of $i\pi T$. Then, the waves

decay on the length $\sim \xi_0$, and, consequently, the loops contribute to equilibrium properties only if the paths are shorter than the coherence length.

Summarizing, we have shown that the quasiclassical technique fails in geometries where classical trajectories form closed loops. In particular, this happens when it is applied to the Josephson multi-layer structure with number of semi-transparent interfaces larger than 2. This conclusion does not undermine the conventional quasiclassical technique but only limits its applicability in some special geometries where the interference of classical paths cannot be neglected. Within the quasiclassical approach, the interference can be incorporated into the theory with the help of the method suggested in Ref. 17.

Acknowledgments

We are grateful to D. Rainer for discussions and critical remarks. This work was supported by the University of Umeå.

-
- * Also at A. F. Ioffe Physico-Technical Institute, 194021 St. Petersburg, Russia.
- ¹ K. K. Likharev, *Rev. Mod. Phys.* **51**, 101 (1979).
 - ² M. Tinkham, *Introduction to Superconductivity*, 2nd ed., (McGraw Hill, N.Y., 1996).
 - ³ G. Eilenberger, *Z. Phys.* **214**, 195 (1968).
 - ⁴ A.I. Larkin and Yu.N. Ovchinnikov, *Zh. Eksp. Teor. Fiz.* **55**, 2262 (1968) [*Sov. Phys. JETP* **28**, 1200 (1969)] A.I. Larkin and Yu.N. Ovchinnikov, in *Nonequilibrium Superconductivity*, ed. D.N. Langenberg and A.I. Larkin, (Elsevier, Amsterdam, 1984).
 - ⁵ A. Schmid in *Nonequilibrium Superconductivity*, ed. K.E. Gray (Plenum, N.Y., 1981).
 - ⁶ J.W. Serene, and D. Rainer, *Phys. Rep.* **4**, 221 (1983).
 - ⁷ Belzig W, Wilhelm F. K, Bruder C, Schon G, and Zaikin A.D, *Superlattices and Microstructures* **25**, 1251 (1999).
 - ⁸ A.L. Shelankov, *Pis'ma Zh. Eksp. Teor. Fiz.* **32**, 122 (1980) [*JETP Lett.* **32**, 111 (1980)].
 - ⁹ G.E. Blonder, M. Tinkham, and T.M. Klapwijk, *Phys. Rev. B* **25**, 4515 (1982).
 - ¹⁰ P. G. de Gennes, *Superconductivity of Metals and Alloys*, (Addison-Wesley, Reading, MA, 1989).
 - ¹¹ A.V. Zaitsev, *Zh. Eksp. Teor. Fiz.* **86**, 1742 (1984), [*Sov. Phys. JETP* **59**, 1015 (1984)].
 - ¹² N. Schopohl and K. Maki, *Phys. Rev. B* **52**, 490 (1995).
 - ¹³ M. Eschrig, *Phys. Rev. B* **61**, 9061 (2000).
 - ¹⁴ A. Shelankov and M. Ozana, *Phys. Rev. B* **61**, 7077 (2000).
 - ¹⁵ T. Lück, U. Eckern, A. Shelankov, *Phys. Rev. B* **63**, 64510 (2001).
 - ¹⁶ M. Ozana, A. Shelankov, in *Proceedings of the Helsinki conference: Symposium on Ultra Low Energy Physics: Methods and Phenomenology*, J. Low Temp. Phys., **124**, 223-243, (2001).
 - ¹⁷ M. Ozana, A. Shelankov, *Phys. Rev. B* **65**, 014510 (2002) (an extended version: cond-mat/0109468).
 - ¹⁸ A. Brinkman and A. A. Golubov, *Phys. Rev. B* **61**, 11297 (2000).
 - ¹⁹ M. Ashida, S. Aoyama, J. Hara, and K. Nagai, *Phys. Rev. B* **40**, 8673 (1989);
 - ²⁰ Proceedings of the Workshop "Quasiclassical Methods of Superconductivity and Superfluidity", Verditz, Austria, March 1996; editors D. Rainer and J. A. Sauls (1998), p. 198.
 - ²¹ In Eq. (1.28), we do not show the factor $(p_+ + p_-)/\sqrt{4p_+p_-}$ which equals to 1 in the main approximation with respect to the small parameter Δ/E_F , E_F being the Fermi energy.
 - ²² A.A. Abrikosov, L.P. Gorkov, and I.E. Dzyaloshinski, *Methods of Quantum Field Theory in Statistical Physics* (Prentice-Hall, Englewood Cliffs, 1963).
 - ²³ K. Fuchs, *Proc. Cambridge Phil. Soc.* **34**, 100 (1938).
 - ²⁴ V. F. Gantmakher, and I. B. Levinson, "Carrier Scattering in Metals and Semiconductors", *Modern Problems in Condensed Matter Sciences*, **19**, North-Holland (1987).
 - ²⁵ One can show that the most general form of \mathcal{D} compatible with the current conservation and the time reversal symmetry is $\mathcal{D} = \begin{pmatrix} a & id \\ ib & c \end{pmatrix}$ where a, b, c , and d are real parameters satisfying the condition $\det \mathcal{D} = 1$.
 - ²⁶ The basis states $\Psi_{\mu}^{(L,R)}$ are ordered as follows. On the left and right, 1: Ψ_{++} , 2: Ψ_{--} , 3: Ψ_{+-} , 4: Ψ_{-+} .

APPENDIX A: THE TRANSFER AND SCATTERING MATRICES

The Bogoliubov - de Gennes equation is a second-order differential equation. In the one-dimensional case considered here, it can be reduced to the first order equation for an "extended" wave functions Ψ which is built of the

wave function ψ and its derivative $\hat{p}\psi$,

$$\Psi(x) = \begin{pmatrix} \psi \\ \hat{p}\psi \end{pmatrix}_x, \quad \hat{p} = -i\frac{d}{dx}. \quad (\text{A1})$$

Since ψ has two components, the extended wave function is a 4-component column.

In terms of Ψ , the quasiparticle current density Eq. (1.6) reads

$$j^{qp} = \frac{1}{2m} \Psi^\dagger \hat{\tau}_z \hat{\sigma}_x \Psi \quad (\text{A2})$$

where σ_x is the Pauli matrix operating in the space $\psi - \hat{p}\psi$, and, as before, $\hat{\tau}_z$ acts in the $u - v$ space.

The charge current Eq. (1.3) can be found as

$$\frac{1}{e} J = \frac{1}{2m} \Psi^\dagger \hat{\sigma}_x \Psi. \quad (\text{A3})$$

The extended wave function corresponding to the plane waves in Eq. (1.11) have the form

$$\Psi_{\nu\sigma}(x) = \sqrt{\frac{m}{\pi}} e^{i\sigma p_\nu x} \Phi_{\nu\sigma} \quad (\text{A4})$$

where the 4-component amplitudes $\Phi_{\nu\sigma}$ may be taken as

$$\Phi_{\nu\sigma} = \frac{1}{\sqrt{2p_\nu}} \begin{pmatrix} \psi_\nu \\ \sigma p_\nu \psi_\nu \end{pmatrix}, \quad (\text{A5})$$

or in a more concise form,

$$\Phi_{\nu\sigma} = \psi_\nu \otimes \phi_{\sigma,p_\nu} \quad (\text{A6})$$

where

$$\phi_{\sigma,p_\nu} = \frac{1}{\sqrt{2p_\nu}} \begin{pmatrix} 1 \\ \sigma p_\nu \end{pmatrix}. \quad (\text{A7})$$

The amplitudes $\Phi_{\nu\sigma}$ are normalized to the probability flux Eq. (A2) equal to $1/2m$ (for $E > |\Delta|$); accordingly, the plane waves in Eq. (A4) are normalised to the δ -function of energy.

The conjugated amplitudes Φ^\dagger defined as

$$\Phi_{\nu\sigma}^\dagger = \psi_\nu^\dagger \otimes \phi_{\sigma,p_\nu}^\dagger \quad \text{where} \quad \phi_{\sigma,p_\nu}^\dagger = \sqrt{\frac{p_\nu}{2}} \begin{pmatrix} 1, \frac{\sigma}{p_\nu} \end{pmatrix}, \quad (\text{A8})$$

($\phi_{\sigma,p}^\dagger = \sigma \phi_{\sigma,p}^T \hat{\sigma}_x$) satisfy the following orthogonality and completeness relations

$$\Phi_{\nu'\sigma'}^\dagger \Phi_{\nu\sigma} = \delta_{\nu'\nu} \delta_{\sigma'\sigma} \quad , \quad \sum_{\nu,\sigma} \Phi_{\nu\sigma} \Phi_{\nu,\sigma}^\dagger = \hat{1}. \quad (\text{A9})$$

Due to the orthogonality property, $\Phi_{\nu,\sigma}^\dagger$ projects a general superposition $\Psi(x)$ to the plane wave $\Psi_{\nu,\sigma}(x)$. Using this argument, one constructs the evolution operator \hat{U}_a , a 4×4 matrix, which relates the wave functions at the points x and $x + a$, $\Psi(x) = \hat{U}_a \Psi(x + a)$,

$$\hat{U}_a = \sum_{\nu,\sigma} e^{-i\sigma p_\nu a} \Phi_{\nu\sigma} \Phi_{\nu\sigma}^\dagger. \quad (\text{A10})$$

In the model where the potential barrier $V(x)$ separating the layers is a δ -function, $V(x) = \frac{\Delta}{m} \delta(x)$, the two-component wave function $\psi(x)$ is continuous at $x = 0$, whereas the derivatives suffer the jump: $\psi'|_{0-}^{0+} = \lambda \psi(0)$. In terms of the extended wave function Ψ Eq. (A1), the interface matching condition reads

$$\Psi_{0-} = \mathcal{D} \Psi_{0+} \quad ; \quad \mathcal{D} = \begin{pmatrix} 1 & 0 \\ 2i\lambda & 1 \end{pmatrix}. \quad (\text{A11})$$

It is implied in Eq. (A11) that each matrix element of \mathcal{D} is multiplied by the unit matrix in the $u - v$ space so that \mathcal{D} is actually a 4×4 matrix.

The transfer matrix, \mathcal{M} , relates the extended wave function, $\Psi^{(L)}$, on the left side of the multi-layer structure to that on the right side $\Psi^{(R)}$:

$$\Psi^{(L)} = \mathcal{M} \Psi^{(R)}. \quad (\text{A12})$$

It is given by the ordered product,

$$\mathcal{M} = \mathcal{D}_1 \mathcal{U}_{1,2} \mathcal{D}_2 \dots \mathcal{U}_{N-1,N} \mathcal{D}_N, \quad (\text{A13})$$

of the matrices \mathcal{D}_k Eq. (A11) corresponding to the k -th interface, $k = 1, \dots, N$, and the evolution matrices $\mathcal{U}_{k,k+1}$ accounting for the propagation from the $k + 1$ -th to k -th potential barrier.

The elements of the S-matrix can be found via the transfer matrix. For this, we take advantage of the completeness relation in Eq. (A9) and present \mathcal{M} as

$$\mathcal{M} = \sum_{\mu,\mu'} \Psi_\mu^{(L)} \mathbf{M}_{\mu\mu'} \Psi_{\mu'}^{\dagger(R)} \quad (\text{A14})$$

where we denote μ the set (ν, σ) and $\mu' = (\nu', \sigma')$. The elements of the matrix \mathbf{M} read

$$\mathbf{M}_{\mu\mu'} = \Psi_\mu^{\dagger(L)} \mathcal{M} \Psi_{\mu'}^{(R)} \quad (\text{A15})$$

where again μ stands for (ν, σ) and $\Psi_{\nu\sigma}$ and $\Psi_{\nu,\sigma}$ are the 4-component amplitudes Eq. (A5) and Eq. (A8), respectively. The meaning of the \mathbf{M} -matrix is that it is the transfer matrix in the plane wave representation: $C_\mu^{(L)} = \sum_{\mu'} \mathbf{M}_{\mu\mu'} C_\mu^{(R)}$ where C 's are the coefficients in the expansion $\Psi^{(L,R)} = \sum_{\mu} C_\mu^{(L,R)} \Psi_\mu^{(L,R)}$.

Presenting \mathbf{M} , found from Eqs. (A13), and (A15), in a block form²⁶,

$$\mathbf{M} = \begin{pmatrix} A & D \\ B & C \end{pmatrix}, \quad (\text{A16})$$

the S -matrix expressed via 2×2 matrices A, B, C , and D , reads

$$S = \begin{pmatrix} B A^{-1} & C - B A^{-1} D \\ A^{-1} & -A^{-1} D \end{pmatrix} \quad (\text{A17})$$

The matrix element S_{kn} gives the amplitude of the scattering from the n -th incoming state listed in Eq. (1.19) to the k -th final state in Eq. (1.20).

APPENDIX B: LOOP CONTRIBUTION

To find contribution of the loops, we first analyze the elementary process that is the scattering on an isolated barrier. Consider a single barrier in between two semi-infinite homogenous superconductors left (L), and right (R). The barrier is characterized by the reflection r and transmission amplitudes t . As required by unitarity, $rt^* + r^*t = 0$ and $R + T = 1$ where $R = |r|^2$, $T = |t|^2$. The free wave functions are listed in Eqs. (1.19), and (1.20).

The scattering matrix calculated by the method described in Appendix A, reads

$$S = \gamma \begin{pmatrix} r\beta\beta^* & |t|^2\alpha^* & t\beta^* & r^*t\alpha^*\beta \\ |t|^2\alpha & r^*\beta\beta^* & t^*r\alpha\beta^* & t^*\beta \\ t\beta & t^*r\alpha^*\beta & r\beta\beta^* & |t|^2\alpha \\ r^*t\alpha\beta^* & t^*\beta^* & \alpha^*|t|^2 & r^*\beta\beta^* \end{pmatrix}. \quad (B1)$$

where

$$\alpha = -\frac{\psi_-^{(R)\dagger}\psi_+^{(L)}}{\psi_-^{(R)\dagger}\psi_-^{(L)}}, \quad \beta = -\frac{1}{\psi_+^{(L)\dagger}\psi_+^{(R)}}, \quad \gamma = \frac{1}{1 - |r|^2\alpha\alpha^*} \quad (B2)$$

Electron ($\psi_+^{(R,L)}$) and hole ($\psi_-^{(R,L)}$) wave functions are defined in Eq. (1.14). By their physical meaning, α is the amplitude of the Andreev reflection on the SS' interface in the absence of barrier, and β is the transmission amplitudes. Outside the energy gap, $\alpha\beta^* + \alpha^*\beta = 0$, $\alpha\alpha^* + \beta\beta^* = 1$ as required by the quasiparticle current conservation. As no surprise, the S-matrix in Eq. (B1) has the same structure as that derived in Ref.8 for the NIS interface.

The loop contribution to the Andreev reflection A_e^{loops} is the sum $A_e^{\text{loops}} = A_e^{(a)} + A_e^{(b)}$ of the processes shown in Fig.10(a) and (b). The amplitudes of each of the processes is the product of factors accumulated along the path. The rules to find the factors are as follows:

(i) The factor which corresponds to the ballistic part of the trajectory is $\exp[i\nu p_\nu |x_f - x_i|]$ where p_ν is the x -component of the momentum Eq. (1.12), $\nu = \pm$ is the type of the excitation (electron, “+”, or hole, “-”), and x_i and x_f is the initial and final value of the x -coordinate. One can prove this formula taking into consideration that the electron propagates in the direction of momentum, and the hole in the opposite direction. (The phase accumulated due to a displacement in the \mathbf{p}_\parallel -direction can be omitted since \mathbf{p}_\parallel is the same for all the ballistic pieces and the path is closed.)

(ii) For an interface scattering event, the factor is the element of the S-matrix corresponding to the initial and final states in Eq. (B1).

Looking at Fig. 10(a,b) and using these rules, one gets

$$A_e^{(a)} = S_{23}^{(1)} e^{ip_+ a_1} S_{14}^{(2)} e^{-ip_- a_2} S_{22}^{(3)} e^{-ip_- a_2} S_{41}^{(2)} e^{ip_+ a_1} S_{31}^{(1)} \\ A_e^{(b)} = S_{24}^{(1)} e^{-ip_- a_1} S_{23}^{(2)} e^{ip_+ a_2} S_{11}^{(3)} e^{ip_+ a_2} S_{32}^{(2)} e^{-ip_- a_1} S_{41}^{(1)}$$

where superscript in $S^{(k)}$, $k = 1, 2, 3$, labels the interface (see Fig.10), and a_1 (a_2) is the distance from the barrier 1 to barrier 2 (from 2 to 3); the momentum p_\pm is calculated for the parameters of the corresponding layer.

Finally, substituting the elements of the S-matrix Eq. (B1), one gets,

$$A_e^{\text{loops}} = A_e^{(a)} + A_e^{(b)} \quad (B3)$$

$$A_e^{\text{loops}} = \mathcal{A} \Re \left(r_1 r_3^* e^{2i(\cos \theta p_F (a_1 - a_2))} \right) \quad (B4)$$

where the coefficient \mathcal{A} reads

$$\mathcal{A} = -\alpha_1 \gamma_1^2 \gamma_2^2 \gamma_3^2 |r_2 t_1 t_2 \alpha_2 \beta_1 \beta_2 \beta_3|^2 e^{2i \frac{\cos \theta}{v_F} (\xi_1 a_1 + \xi_2 a_2)}. \quad (B5)$$

Here, θ is the angle between the direction of the trajectory and the x -axis, and $\xi_{1,2}$ is defined by Eq. (1.13) for the corresponding layer.